

## MODEL X-RAY SPECTRA OF MAGNETIC NEUTRON STARS WITH HYDROGEN ATMOSPHERES

WYNN C. G. HO

Harvard-Smithsonian Center for Astrophysics, 60 Garden St., Cambridge, MA, 02138, USA  
wynnho@slac.stanford.edu

AND

ALEXANDER Y. POTEKHIN<sup>1</sup>

Ioffe Physico-Technical Institute, Politeknicheskaya 26, 194021 St. Petersburg, Russia  
palex@astro.ioffe.ru

AND

GILLES CHABRIER

Ecole Normale Supérieure de Lyon, CRAL (UMR CNRS No. 5574), 69364 Lyon Cedex 07, France  
chabrier@ens-lyon.fr

Draft version November 12, 2018

### ABSTRACT

We construct partially ionized hydrogen atmosphere models for magnetized neutron stars in radiative equilibrium with fixed surface fields between  $B = 10^{12}$  and  $2 \times 10^{13}$  G and effective temperatures  $\log T_{\text{eff}} = 5.5\text{--}6.8$ , as well as with surface  $B$  and  $T_{\text{eff}}$  distributions around these values. The models are based on the latest equation of state and opacity results for magnetized, partially ionized hydrogen plasmas. The atmospheres directly determine the characteristics of thermal emission from the surface of neutron stars. We also incorporate these model spectra into XSPEC, under the model name NSMAX, thus allowing them to be used by the community to fit X-ray observations of neutron stars.

*Subject headings:* radiative transfer – stars: atmospheres – stars: magnetic fields – stars: neutron – X-rays: stars

### 1. INTRODUCTION

Thermal radiation has been detected from radio pulsars and radio-quiet neutron stars (NSs; see Kaspi, Roberts, & Harding 2006; Haberl 2007; van Kerkwijk & Kaplan 2007; Zavlin 2007, for reviews) and from soft gamma-ray repeaters and anomalous X-ray pulsars, which form the magnetar class of NSs endowed with superstrong ( $B \gtrsim 10^{14}$  G) magnetic fields (see Woods & Thompson 2006, for a review). Radiation from the surface of these NSs can provide invaluable information on the physical properties and evolution of the NSs. Characteristics of the NS, such as the gravitational mass  $M$ , circumferential radius  $R$ , and surface temperature  $T$ , depend on the poorly constrained physics of the stellar interior, such as the nuclear equation of state (EOS) and quark and superfluid/superconducting properties at supra-nuclear densities. Many NSs are also known to possess strong magnetic fields ( $B \sim 10^{12}\text{--}10^{13}$  G), with some well above the quantum critical value ( $B \gg B_Q = 4.414 \times 10^{13}$  G).

The observed radiation from a NS originates in a thin atmospheric layer (with scale height  $\sim 1$  cm) that covers the stellar surface. To properly interpret the observations of NS surface emission and to provide accurate constraints on the physical properties of NSs, it is important to understand in detail the radiative behavior of NS atmospheres in the presence of strong magnetic fields. The properties of the atmosphere, such as the chemical composition, EOS, and radiative opacities, directly determine the characteris-

tics of the observed spectrum. While the surface composition of the NS is unknown, a great simplification arises due to the efficient gravitational separation of light and heavy elements (see Alcock & Illarionov 1980; Brown, Bildsten, & Chang 2002). A pure hydrogen atmosphere is expected even if a small amount of fallback/accretion occurs after NS formation; the total mass of hydrogen needed to form an optically thick atmosphere can be less than  $\sim 10^{16}$  g. Alternatively, a helium atmosphere may be possible as a result of diffusive hydrogen burning on the NS surface (Chang & Bildsten 2003; Chang, Arras, & Bildsten 2004). Finally, a heavy element atmosphere may exist if no accretion takes place or if all the accreted matter is consumed by thermonuclear reactions.

Steady progress has been made in modeling NS atmospheres (see Pavlov et al. 1995; Ho & Lai 2001, 2003; Zavlin 2007, for more detailed discussion and references on NS atmosphere modeling). Since the NS surface emission is thermal in nature, it has been modeled at the lowest approximation with a blackbody spectrum. Early works on atmospheric spectra assume emission from light element, unmagnetized atmospheres (the latter assumption being valid for  $B \lesssim 10^9$  G); computed spectra exhibit significant deviation from a Planckian shape and distinctive hardening with respect to a blackbody (Romani 1987; Rajagopal & Romani 1996; Zavlin, Pavlov, & Shibano 1996; Gänsicke, Braje, & Romani 2002).

The strong magnetic fields present in NS atmospheres significantly increase the binding energies of atoms, molecules, and other bound states (see, e.g., Lai 2001, for a review). Abundances of these bound states can be ap-

<sup>1</sup> Also at the Isaac Newton Institute of Chile (St. Petersburg Branch), St. Petersburg, Russia

preciable in the atmospheres of cold NSs (i.e., those with surface temperature  $T \lesssim 10^6$  K; Lai & Salpeter 1997; Potekhin, Chabrier, & Shibano 1999). In addition, the presence of a magnetic field causes emission to be anisotropic (Pavlov et al. 1994; Zavlin et al. 1995a) and polarized (Mészáros et al. 1988; Pavlov & Zavlin 2000); this must be taken into account self-consistently when developing radiative transfer codes. The most comprehensive early studies of magnetic NS atmospheres focused on a fully ionized hydrogen plasma and moderate field strengths ( $B \sim 10^{12}$ – $10^{13}$  G; Miller 1992; Shibano et al. 1992; Pavlov et al. 1994; Zane, Turolla, & Treves 2000). These models are expected to be valid only for relatively high temperatures ( $T \gtrsim$  a few  $\times 10^6$  K), where hydrogen is almost completely ionized. More recently, atmosphere models in the ultra-strong field ( $B \gtrsim 10^{14}$  G) and relevant temperature regimes have been presented (Ho & Lai 2001, 2003; Özel 2001; Zane et al. 2001; Lloyd 2003; van Adelsberg & Lai 2006; see Bezchastnov et al. 1996; Bulik & Miller 1997, for early work), and all of these rely on the assumption of a fully ionized hydrogen composition (see, however, Ho et al. 2003). Magnetized non-hydrogen atmospheres have been studied by Miller (1992) and Rajagopal, Romani, & Miller (1997), but because of the complexity of the atomic physics, the models were necessarily crude (see Mori & Ho 2007, for more details). Only recently have self-consistent atmosphere models (Ho et al. 2003; Potekhin et al. 2004; Mori & Ho 2007) using the latest EOS and opacities for partially ionized hydrogen (Potekhin & Chabrier 2003, 2004) and mid- $Z$  elements (Mori & Hailey 2002, 2006) been constructed.

Here we present a systematic tabulation of our partially ionized hydrogen atmosphere models for  $B = 10^{12}$ – $2 \times 10^{13}$  G. We incorporate these tables into XSPEC<sup>2</sup> (Arnaud 1996), under the model name NSMAX, for use by the astronomical community. Note that the NS atmosphere models previously implemented in XSPEC are either non-magnetic (NSAGRAV: Zavlin et al. 1996; NSSPEC: Gänsicke et al. 2002; NSATMOS: McClintock, Narayan, & Rybicki 2004; Heinke et al. 2006) or magnetic but fully ionized hydrogen (NSA: Pavlov et al. 1995); the last at two fields:  $B = 10^{12}$  G and  $10^{13}$  G. In § 2, we give details on the construction of the atmosphere models. In § 3, we present our results, and we summarize and mention future work in § 4.

## 2. CONSTRUCTION OF ATMOSPHERE MODEL

Thermal radiation from the surface of a NS is mediated by the stellar atmosphere. The model for emission through the atmosphere is constructed using a grid in Thomson depth  $\tau$ , photon energy  $E$ , and photon propagation direction  $(\theta_k, \phi_k)$ , where  $\theta_k$  is the angle between the photon wave-vector  $\mathbf{k}$  and the surface normal  $\mathbf{n}$  and  $\phi_k$  is the azimuthal angle between  $\mathbf{k}$  and the magnetic field  $\mathbf{B}$  (see Fig. 1). Grid intervals are equally spaced logarithmically for depth  $10^{-5} \lesssim \tau \lesssim 10^3$  and energy  $0.01 \lesssim E \lesssim 10$  keV and spaced every  $5^\circ$  for  $\theta_k$  and  $10^\circ$  for  $\phi_k$  (extra grid points are included around  $\theta_k = \Theta_B$ , where  $\Theta_B$  is the angle between  $\mathbf{n}$  and  $\mathbf{B}$ ); 6 grid points

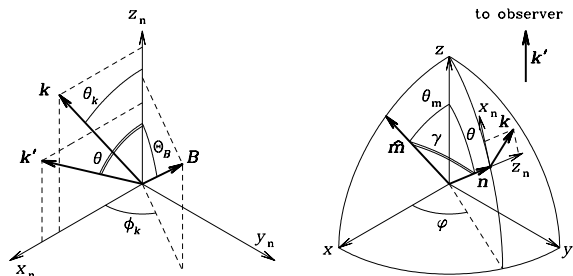


FIG. 1.— Coordinate axes and angles used to describe the atmosphere model. Two Cartesian coordinate frames,  $(x_n y_n z_n)$  and  $(xyz)$ , are considered. The  $z_n$ -axis is directed along the surface normal  $\mathbf{n}$ .  $\mathbf{B}$  is the magnetic field, and  $\Theta_B$  and  $\phi_k$  are its polar and azimuthal angles in the  $(x_n y_n z_n)$ -frame.  $\mathbf{k}$  is the photon wave-vector at the surface and lies in the  $(x_n z_n)$ -plane,  $\theta_k$  is the angle between  $\mathbf{k}$  and  $\mathbf{n}$ , and  $\mathbf{k}'$  is the photon wave-vector at infinity and is directed along  $z$  ( $\mathbf{k} = \mathbf{k}'$  in the absence of gravitational light-bending).  $\theta$  and  $\varphi$  are the polar and azimuthal angles of the surface point at the stellar surface in the  $(xyz)$ -frame (clearly, the angle between  $\mathbf{n}$  and  $\mathbf{k}'$  equals  $\theta$ ). For a magnetic dipole,  $\mathbf{m}$  is the unit vector along the magnetic axis, which lies in the  $(xz)$ -plane,  $\theta_m$  is the angle between  $\mathbf{k}'$  and  $\mathbf{m}$ , and  $\gamma$  is the magnetic colatitude of the surface point.

are used per decade in  $\tau$ , and 50 grid points are used per decade in  $E$ . Under typical conditions in NS atmospheres with  $B \gtrsim 10^{12}$  G, radiation propagates in two polarization modes (see, e.g., Mészáros 1992); therefore, the radiative transfer equations for the two coupled modes are solved to determine the emission properties of a magnetic atmosphere. The self-consistency of the atmosphere model is determined by requiring that the deviations (at each Thomson depth) from radiative equilibrium and constant total flux are  $\ll 1\%$  and  $\lesssim 0.5\%$ , respectively (see Ho & Lai 2001; Ho et al. 2003; Potekhin et al. 2004, and references therein for details on the construction of the atmosphere models). The atmosphere models mainly depend on three parameters: the effective temperature  $T_{\text{eff}}$  and the magnetic field strength  $B$  and inclination  $\Theta_B$  (see Fig. 1). The atmosphere models also have a dependence, through hydrostatic balance, on the surface gravity  $g = (1 + z_g) GM/R^2 \approx 1.328 \times 10^{14} (1 + z_g) (M/M_\odot) (R/10 \text{ km})^{-2} \text{ cm s}^{-2}$ , where  $z_g$  is the gravitational redshift,  $1 + z_g = (1 - r_g/R)^{-1/2}$ , and  $r_g = 2GM/c^2 \approx 2.95 (M/M_\odot) \text{ km}$  is the gravitational radius. Thus the atmosphere model depends on the NS mass  $M$  and radius  $R$ ; however, the resulting spectra do not vary significantly for different values of  $g$  around  $2 \times 10^{14} \text{ cm s}^{-2}$  (Pavlov et al. 1995; see Figs. 4, 8, and 9).

The spectra from models constructed as discussed above only describe emission from either a local patch of the stellar surface with the particular  $T_{\text{eff}}$  and  $\mathbf{B}$  or a star with a uniform temperature and radial magnetic field of uniform strength at the surface. By taking into account surface magnetic field and temperature distributions, we can construct more physical models of emission from NSs; however these spectra from the whole NS surface are necessarily model-dependent, as the  $\mathbf{B}$  and  $T$  distributions are generally unknown (see, e.g., Zavlin et al. 1995a; Zane et al. 2001; Ho & Lai 2004; Pérez-Azorín et al. 2006; Zane & Turolla 2006; Ho 2007; see also Geppert, Küker, & Page 2006; Aguilera, Pons, & Miralles 2007;

<sup>2</sup> <http://heasarc.gsfc.nasa.gov/docs/xanadu/xspec/>

TABLE 1  
MAGNETIC FIELD DISTRIBUTION OF NEUTRON STAR SURFACE

$\gamma$ (deg)	$\Theta_B$ (deg)	$B$ ( $10^{12}$ G)	
		case 1	case 2
0	0	10	1.82
30	20	9	1.65
60	45	7	1.26
90	90	5.5	1

Potekhin, Chabrier, & Yakovlev 2007; Reisenegger et al. 2007, and references therein, for recent work on surface  $B$  and  $T$  distributions). Therefore, we provide results from two sets of models: one set with a single  $B$  and  $T_{\text{eff}}$ , as has been done previously for NS atmospheres with fully ionized hydrogen (see NSA; Pavlov et al. 1995), and a set which is constructed with  $B$  and  $T_{\text{eff}}$  varying across the surface. The latter is built by dividing the surface into regions with different  $B$  and  $T_{\text{eff}}$ . Relatively simple distributions are adopted (see Tables 1 and 2). In particular, we assume a dipolar magnetic field, after accounting for the effect of General Relativity, such that the surface distribution of  $B$  is given by

$$B = (B_{\text{pole}}/2)[(2 + f)(\mathbf{n} \cdot \hat{\mathbf{m}})\mathbf{n} - f\hat{\mathbf{m}}] \quad (1)$$

(Ginzburg & Ozernoi 1965; see also Pavlov & Zavlin 2000), where  $B_{\text{pole}}$  is the field strength at the magnetic pole,  $f = f(M/R) > 1$  accounts for spatial curvature ( $f = 1$  in planar geometry), and  $\hat{\mathbf{m}}$  is the direction of the magnetic moment. The surface temperature distribution is calculated using the results of Potekhin et al. (2003) for the “canonical” NS mass  $M = 1.4M_{\odot}$  and the radius  $R = 12$  km, corresponding to moderately stiff NS EOSs (see, e.g., Haensel, Potekhin, & Yakovlev 2007). In order to minimize model dependence, we assume the  $T_{\text{eff}}$ -distribution of an iron heat-blanketing envelope. This assumption does not change our results since, for any chemical composition of the envelope, the dependence of  $T_{\text{eff}}$  on the magnetic colatitude  $\gamma$  is similar to that given in Greenstein & Hartke (1983) (see Potekhin et al. 2003).

Emission from any point along a circle at a fixed  $\gamma$  is given by the atmosphere model for that  $\gamma$ . Using equation (1) and the coordinate transformation

$$\begin{aligned} \hat{\mathbf{x}}_n &= -\cos\varphi\cos\theta\hat{\mathbf{x}} - \sin\varphi\cos\theta\hat{\mathbf{y}} + \sin\theta\hat{\mathbf{z}} \\ \hat{\mathbf{y}}_n &= -\sin\varphi\hat{\mathbf{x}} - \cos\varphi\hat{\mathbf{y}} \\ \hat{\mathbf{z}}_n &= \cos\varphi\sin\theta\hat{\mathbf{x}} + \sin\varphi\sin\theta\hat{\mathbf{y}} + \cos\theta\hat{\mathbf{z}}, \end{aligned} \quad (2)$$

where  $\theta$  and  $\varphi$  are the polar and azimuthal angles of  $\mathbf{n}$  with respect to the line of sight (see Fig. 1) and  $(\hat{\mathbf{x}}, \hat{\mathbf{y}}, \hat{\mathbf{z}})$  and  $(\hat{\mathbf{x}}_n, \hat{\mathbf{y}}_n, \hat{\mathbf{z}}_n)$  are the unit coordinate vectors for frames  $(x, y, z)$  and  $(x_n, y_n, z_n)$ , respectively, one finds that

$$\cos\gamma = \cos\varphi\sin\theta\sin\theta_m + \cos\theta\cos\theta_m, \quad (3)$$

$$\sin\phi_k = \sin\varphi\sin\theta_m/\sin\gamma, \quad (4)$$

$$B = B_{\text{pole}}\sqrt{\cos^2\gamma + (f/2)^2\sin^2\gamma}, \quad (5)$$

$$\tan\Theta_B = (f/2)\tan\gamma, \quad (6)$$

where  $\theta_m$  is the angle between  $\hat{\mathbf{m}}$  and  $\mathbf{k}'$  and  $\phi_k = \varphi$  in the special case  $\gamma = 0$ . The photon wave-vector at infinity  $\mathbf{k}'$  differs from  $\mathbf{k}$  at

TABLE 2  
EFFECTIVE TEMPERATURES  $T_{\text{eff}}/(10^5$  K) OF NEUTRON STAR ATMOSPHERE MODELS

$\log T_{\text{eff}}^{\text{NS}}$	$\Theta_B$			
	$0^\circ$	$20^\circ$	$45^\circ$	$90^\circ$
	$B$ ( $10^{12}$ G)			
	1.82	1.65	1.26	1
5.5	3.8	3.7	3.2	0.55 <sup>a</sup>
5.6	4.7	4.6	4.0	0.82 <sup>a</sup>
5.7	6.0	5.8	5.1	1.2 <sup>a</sup>
5.8	7.5	7.3	6.4	1.8 <sup>a</sup>
5.9	9.4	9.2	8.0	2.66
6.0	12	11.5	10	3.9
6.1	15	14	13	5.66
6.2	19	18	16	8.1
6.3	23.3	22.8	20	11.6
6.4	29	28	25	16
6.5	36	35	32	22.3
6.6	45	44	40	30.4
6.7	56	55	50	40.7
6.8	70	69	63	54
	$B$ ( $10^{12}$ G)			
	10	9	7	5.5
5.5	3.75	3.66	3.2	0.27 <sup>a</sup>
5.6	4.7	4.6	4.04	0.4 <sup>a</sup>
5.7	5.94	5.8	5.1	0.59 <sup>a</sup>
5.8	7.5	7.3	6.4	0.86 <sup>a</sup>
5.9	9.47	9.2	8.0	1.3 <sup>a</sup>
6.0	12	11.6	10	1.9 <sup>a</sup>
6.1	15	14.6	12.7	2.9
6.2	19	18.3	16	4.4
6.3	23.6	23	20	6.5
6.4	29.6	29	25.5	9.5
6.5	37	36	32	13.8
6.6	46.6	46	40	19.8
6.7	58.4	57	51	28
6.8	73	72	64	39

NOTE. — Models assume  $g = 1.6 \times 10^{14}$  cm s<sup>-2</sup>. <sup>a</sup>Spectra for these temperatures use blackbodies with  $T = T_{\text{eff}}$ .

the surface due to gravitational redshift and light-bending (Pechenick, Ftaclas, & Cohen 1983; Page 1995; Pavlov & Zavlin 2000). The latter is taken into account by making use of the approximation from Beloborodov (2002) (see also Zavlin, Shibunov, & Pavlov 1995b),

$$1 - \cos\theta = (1 - \cos\theta_k)/(1 - r_g/R). \quad (7)$$

The spectrum for the entire surface is then computed by summing over the emission from different regions,

$$F_E = A \int_0^{2\pi} d\varphi \int_0^{\pi/2} \sin\theta_k d\theta_k I_E(\theta_k, \phi_k; B, \Theta_B), \quad (8)$$

where  $I_E$  is the specific intensity. Note that  $E$  is the unredshifted photon energy. The explicit redshifting of the photon energy and flux spectrum is not done at this stage, though relativistic effects are taken into account [see, e.g., eqs. (5) and (7)]; redshifting is done in the

XSPEC fitting code (see § 3). At this point in the model calculation, the flux normalization  $A$  [=  $A(M, R, d)$ , where  $d$  is the distance to the source] is taken to be unity (see § 3 for discussion of its model-dependence).

We calculate  $I_E$  for four  $\gamma$  values (see Table 1) and perform the integration in equation (8) by interpolating between the calculated values. For  $T_{\text{eff}}(\gamma = 90^\circ) < 2 \times 10^5$  K, we use blackbody spectra at  $T = T_{\text{eff}}$  (see Table 2); the spectral contributions at these temperatures contribute little to the total X-ray spectra [since  $T_{\text{eff}}^{\text{NS}} \gg T_{\text{eff}}(\gamma = 90^\circ)$ ; replacing the blackbody spectrum with zero values yields no appreciable difference in the resulting integrated spectrum], which is dominated by emission from the hotter regions of the NS surface. Strong absorption features, such as the proton cyclotron line at  $E_{Bp} = \hbar e B / m_p c$ , are broadened due to the variation of  $B$  with  $\gamma$ . In order to reproduce this broadening in our interpolation, we first remap our calculated  $I_E$  as a function of  $E/E_{Bp}$ :  $I_E(\theta_k, \phi_k; B, \Theta_B) \equiv \tilde{I}(E/E_{Bp}, \theta_k, \phi_k; \gamma)$ . We then interpolate  $\tilde{I}$  in  $\theta_k$ ,  $\phi_k$ , and  $B(\gamma)$  for every fixed  $E/E_{Bp}$  and substitute the resulting  $I_E$  into equation (8).

### 3. RESULTS

For the first set of models (with uniform  $B$  and  $T_{\text{eff}}$ ), we consider  $g = 1.6$  and  $2.4 \times 10^{14}$  cm s $^{-2}$ ; for a NS with  $M = 1.4M_\odot$ , this corresponds to  $R = 12$  km and 10 km, respectively. The magnetic field is  $B = 10^{12}$ ,  $1.26 \times 10^{12}$ ,  $2 \times 10^{12}$ ,  $4 \times 10^{12}$ ,  $7 \times 10^{12}$ ,  $10^{13}$ , or  $2 \times 10^{13}$  G and  $\Theta_B = 0^\circ$ . The effective temperatures span the range  $\log T_{\text{eff}} = 5.5$ –6.8 (5.6–6.8 for  $B = 2 \times 10^{13}$  G) with the temperature interval between each model  $\Delta \log T_{\text{eff}} \approx 0.1$ . The temperature and abundance profiles for the atmosphere models with  $g = 2.4 \times 10^{14}$  cm s $^{-2}$  and  $B = 10^{12}$  G and  $10^{13}$  G are shown in Figures 2 and 3, respectively. The atomic fraction is the number of hydrogen atoms with non-destroyed energy levels divided by the total number of protons (Potekhin & Chabrier 2003). Here we only account for the ground-state atoms, which substantially reduces the computational work. This approximation is justified because the fraction of atoms in excited states is small in most of the considered temperature profiles: it does not exceed a few percent even when the abundance of ground-state atoms reaches tens of percent. The dependence of the atomic fraction on temperature and magnetic field is clear: lower temperatures or higher magnetic fields increase the abundance of bound species. The dependence on density is more complex: an increase in the atomic fraction with growing density (recombination according to the modified Saha equation) competes with the decrease due to pressure ionization, which ultimately turns to complete ionization at high  $\rho$ .

Figures 4–10 show the (unredshifted) spectra for  $B = 10^{12}$ ,  $1.26 \times 10^{12}$ ,  $2 \times 10^{12}$ ,  $4 \times 10^{12}$ ,  $7 \times 10^{12}$ ,  $10^{13}$ , and  $2 \times 10^{13}$  G. The most prominent spectral features are due to the proton cyclotron line at  $E_{Bp} = 0.063(B/10^{13}$  G) keV, the  $s = 0 \rightarrow 1$  transition at  $E = 0.051$  keV for  $B = 10^{12}$  G and 0.14 keV for  $10^{13}$  G, the  $s = 0 \rightarrow 2$  transition at 0.075 keV for  $10^{12}$  G and 0.23 keV for  $10^{13}$  G, and the peak of the bound-free transition at 0.16 keV for  $10^{12}$  G and 0.31 keV for  $10^{13}$  G. Here  $s$  is the quantum number that measures transverse atomic excitations and corresponds to the projection of the angular momentum onto the magnetic field lines,

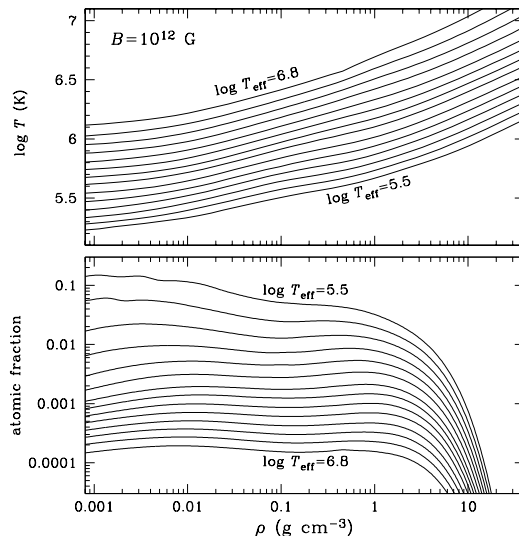


FIG. 2.— Temperature and abundance profiles at various  $T_{\text{eff}}$  of a partially ionized hydrogen atmosphere with  $B = 10^{12}$  G,  $\Theta_B = 0^\circ$ , and  $g = 2.4 \times 10^{14}$  cm s $^{-2}$ .

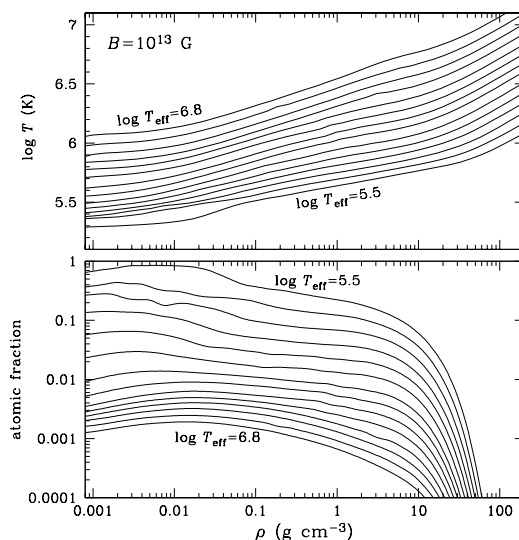


FIG. 3.— Temperature and abundance profiles at various  $T_{\text{eff}}$  of a partially ionized hydrogen atmosphere with  $B = 10^{13}$  G,  $\Theta_B = 0^\circ$ , and  $g = 2.4 \times 10^{14}$  cm s $^{-2}$ .

whereas the longitudinal and Landau quantum numbers equal zero for the bound states involved in these transitions (see Potekhin 1994, for a detailed description of the quantum numbers of a moving hydrogen atom). All the spectral features due to atomic transitions are substantially broadened because of the “motional Stark effect” (see, e.g., Potekhin & Pavlov 1997, and references therein). This “magnetic broadening” becomes stronger with increasing  $T$  and is another reason, in addition to the decrease in the neutral fraction, for the disappearance of the features from the spectra at higher  $T_{\text{eff}}$ .

For the second set of models, we take  $g = 1.6 \times 10^{14}$  cm s $^{-2}$ . The range of magnetic fields and effective temperatures ( $B, \Theta_B, T_{\text{eff}}$ ) of the models are given in Table 2. These values correspond to a magnetic dipole model of a NS with  $R = 12$  km and  $M = 1.4M_\odot$ , in

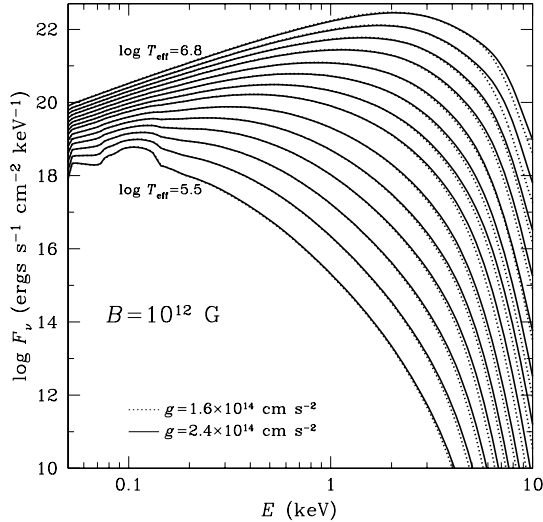


FIG. 4.— Spectra at various  $T_{\text{eff}}$  of a partially ionized hydrogen atmosphere with  $B = 10^{12}$  G and  $\Theta_B = 0^\circ$ . Dotted and solid lines are for  $g = 1.6$  and  $2.4 \times 10^{14}$   $\text{cm s}^{-2}$ , respectively.

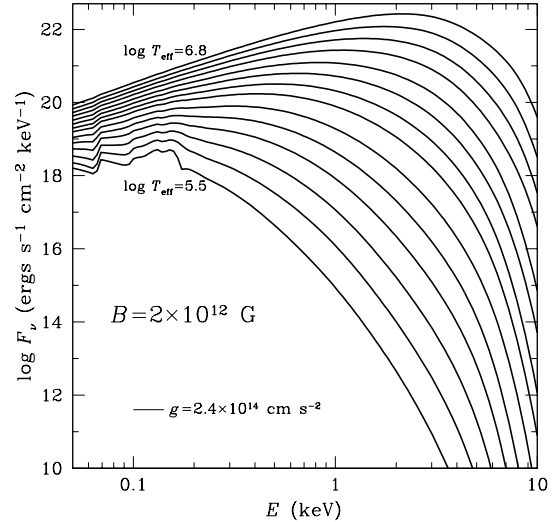


FIG. 6.— Spectra at various  $T_{\text{eff}}$  of a partially ionized hydrogen atmosphere with  $B = 2 \times 10^{12}$  G,  $\Theta_B = 0^\circ$ , and  $g = 2.4 \times 10^{14}$   $\text{cm s}^{-2}$ .

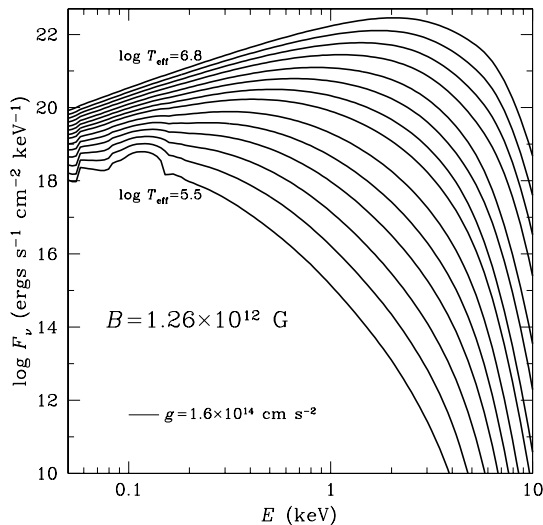


FIG. 5.— Spectra at various  $T_{\text{eff}}$  of a partially ionized hydrogen atmosphere with  $B = 1.26 \times 10^{12}$  G,  $\Theta_B = 0^\circ$ , and  $g = 1.6 \times 10^{14}$   $\text{cm s}^{-2}$ .

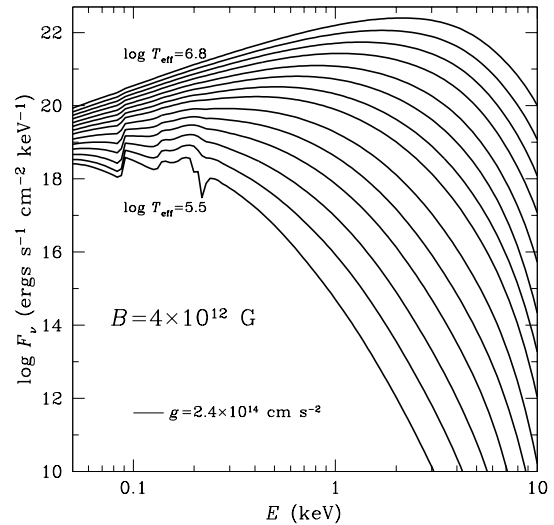


FIG. 7.— Spectra at various  $T_{\text{eff}}$  of a partially ionized hydrogen atmosphere with  $B = 4 \times 10^{12}$  G,  $\Theta_B = 0^\circ$ , and  $g = 2.4 \times 10^{14}$   $\text{cm s}^{-2}$ .

agreement with the chosen  $g$ . One subset of models has  $B = 10^{12}$  G at the magnetic equator, while the other has  $B = 10^{13}$  G at the pole.  $T_{\text{eff}}^{\text{NS}}$  is the mean effective temperature for the whole NS, which corresponds to the total heat flux from the surface (see, e.g., Potekhin et al. 2003). For each  $T_{\text{eff}}^{\text{NS}}$ , the spectra are calculated as described in § 2 and using equation (8). The resulting spectra are shown in Figures 11–14 for the cases  $\theta_m = 0$  and  $90^\circ$ . For comparison, the dotted lines show the atmosphere spectra for a uniform surface temperature and radial magnetic field (see Figs. 4 and 9). We see that the field distribution over the stellar surface substantially smears the spectral features from atomic transitions. This smearing is especially noticeable in Figures 13 and 14, where the atomic features are stronger due to the higher atomic fractions.

Finally, we supply XSPEC, under the model name NSMAX, with tables of the spectra shown in Figures 4–14, as well as a code to interpolate within each table; note that the model spectra with single  $(B, T_{\text{eff}})$ -values span the photon energy range  $0.05 \lesssim E \lesssim 10$  keV, while the model spectra with  $(B, T_{\text{eff}})$ -distributions cover  $0.09 \lesssim E \lesssim 5$  keV. The code first unredshifts the energy bins of the observed spectrum, then obtains the fit spectrum by linear interpolation via a weighted average of the nearest two model  $\log T_{\text{eff}}$  and  $E$ , and finally redshifts the fit spectrum by  $(1 + z_g)^{-1}$ . The code requires one switch parameter and two fit parameters ( $\log T_{\text{eff}}$  and  $1 + z_g$ ); XSPEC automatically adds a third fit parameter (normalization  $A$ ). The switch parameter indicates which table of model spectra to use: the differences being due to the composition (only hydrogen at the present

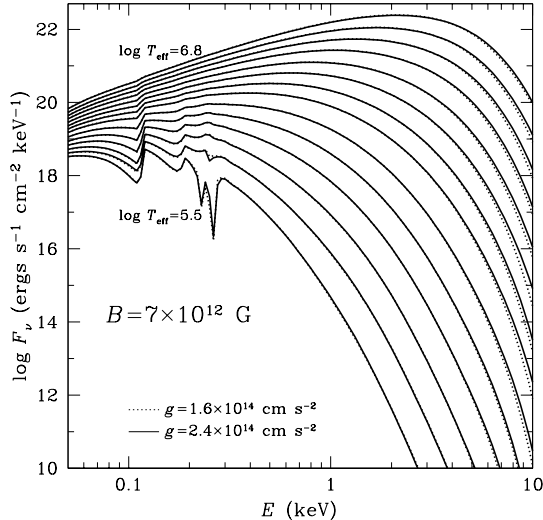


FIG. 8.— Spectra at various  $T_{\text{eff}}$  of a partially ionized hydrogen atmosphere with  $B = 7 \times 10^{12}$  G and  $\Theta_B = 0^\circ$ . Dotted and solid lines are for  $g = 1.6$  and  $2.4 \times 10^{14}$  cm s $^{-2}$ , respectively.

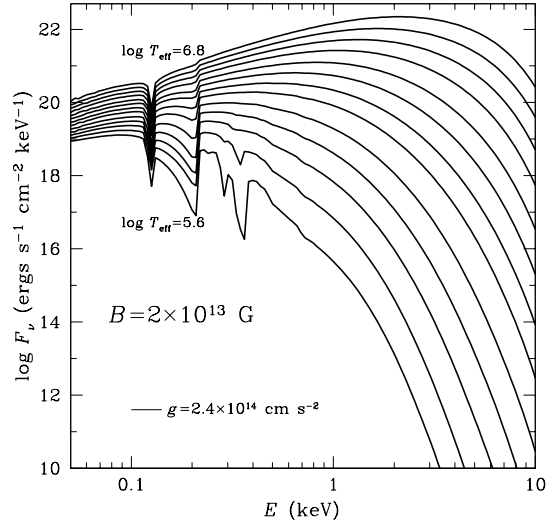


FIG. 10.— Spectra at various  $T_{\text{eff}}$  of a partially ionized hydrogen atmosphere with  $B = 2 \times 10^{13}$  G,  $\Theta_B = 0^\circ$ , and  $g = 2.4 \times 10^{14}$  cm s $^{-2}$ .

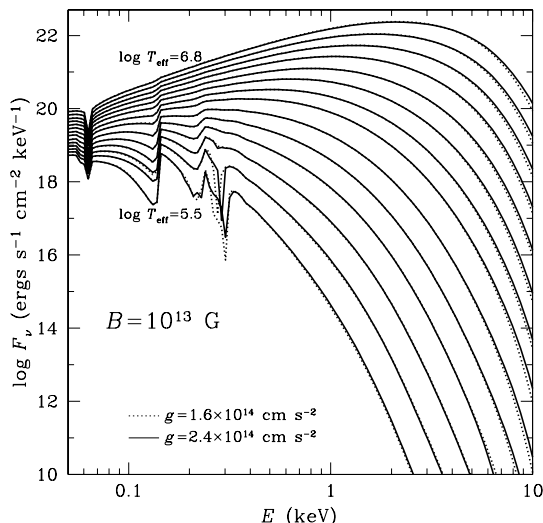


FIG. 9.— Spectra at various  $T_{\text{eff}}$  of a partially ionized hydrogen atmosphere with  $B = 10^{13}$  G and  $\Theta_B = 0^\circ$ . Dotted and solid lines are for  $g = 1.6$  and  $2.4 \times 10^{14}$  cm s $^{-2}$ , respectively.

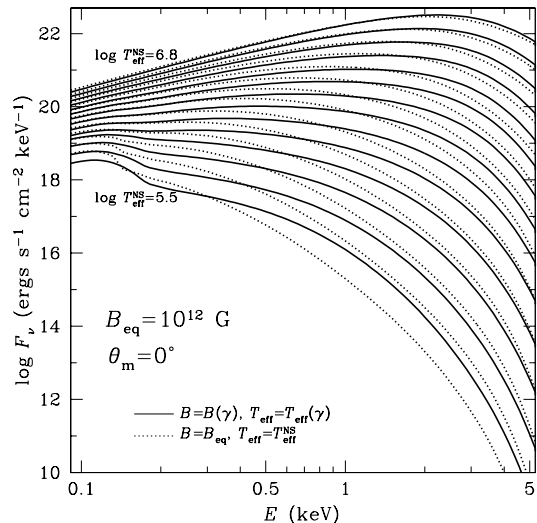


FIG. 11.— Spectra at various total NS  $T_{\text{eff}}^{\text{NS}}$  of a partially ionized hydrogen atmosphere covering a NS with  $R = 12$  km and  $M = 1.4M_\odot$ , surface distributions of  $\mathbf{B}$  and  $T_{\text{eff}}$  according to the magnetic dipole model (see Tables 1 and 2;  $B_{\text{pole}} = 1.82 \times 10^{12}$  G and  $B = 10^{12}$  G at the magnetic equator), and  $\theta_m = 0$ . Dotted lines correspond to atmosphere spectra with a uniform temperature ( $T_{\text{eff}} = T_{\text{eff}}^{\text{NS}}$ ) and uniform radial magnetic field  $B = 10^{12}$  G.

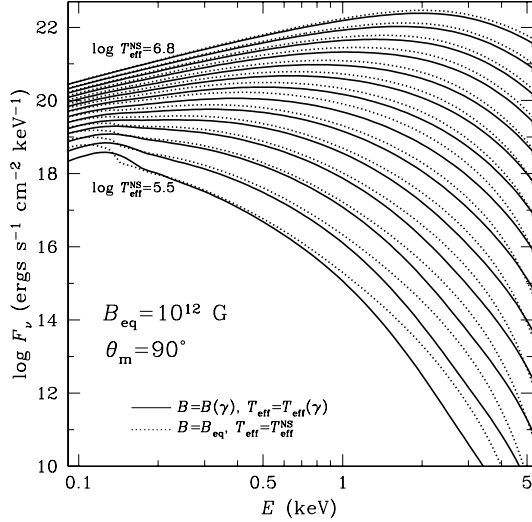
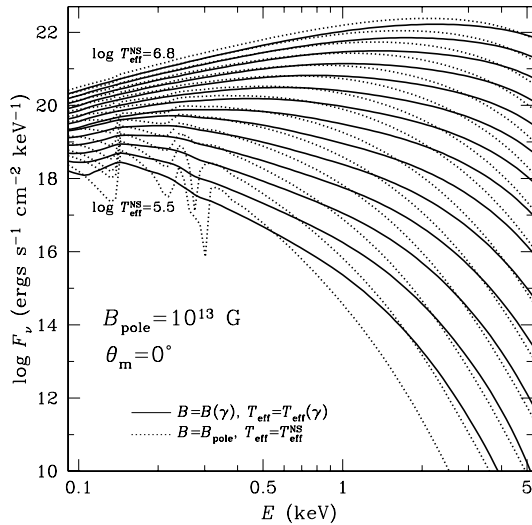
time; see § 4),  $B$ ,  $\Theta_B$ , and  $g$  for the first set of models and the composition,  $B$ ,  $\theta_m$ , and  $g$  for the second set of models. The normalization parameter  $A$  is conventionally taken to be equal to  $(R^\infty/d)^2/(1+z_g)^3$ , where  $R^\infty = R(1+z_g)$ , and the same  $R$  is used to calculate  $z_g$ ; note that this prescription implies the emission region is the entire visible surface of the NS.

#### 4. SUMMARY

We have constructed tables of model atmosphere spectra for neutron stars (with magnetic fields  $B = 10^{12}$ – $2 \times 10^{13}$  G and effective temperatures  $\log T_{\text{eff}} = 5.5$ – $6.8$ ) and incorporated these tables into XSPEC (under the model name NSMAX<sup>3</sup>). These spectra are ob-

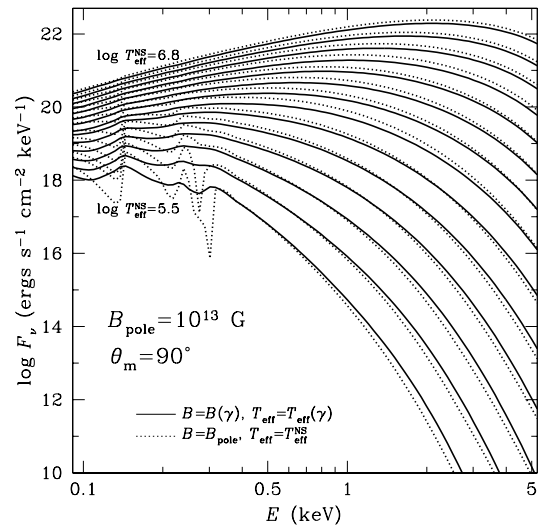
tained using the most up-to-date equation of state and opacities for a partially ionized hydrogen plasma, and therefore they can describe emission from neutron stars with surface temperatures  $T \lesssim 10^6$  K, where the abundance of bound species is appreciable, as well as neutron stars with  $T > 10^6$  K. Thus we go beyond the previous magnetic neutron star spectral models provided in XSPEC, which assume fully ionized hydrogen atmospheres. Our implementation in XSPEC allows easy updates to the database of model spectra, so that tables of models with other magnetic field strengths (e.g., other than the seven fields,  $B = 10^{12}$ ,  $1.26 \times 10^{12}$ ,  $2 \times 10^{12}$ ,

<sup>3</sup> <http://heasarc.gsfc.nasa.gov/docs/xanadu/xspec/models/nsmax.html>

FIG. 12.— The same as in Fig. 11 but with  $\theta_m = 90^\circ$ .FIG. 13.— The same as in Fig. 11 but with  $B_{\text{pole}} = 10^{13}$  G and  $B = 5.5 \times 10^{12}$  G at the equator. Dotted lines correspond to atmosphere spectra with a uniform radial magnetic field  $B = 10^{13}$  G.

$4 \times 10^{12}$ ,  $7 \times 10^{12}$ ,  $10^{13}$ , and  $2 \times 10^{13}$  G, currently provided) or other elements (e.g., carbon, oxygen, and neon; see Mori & Ho 2007) will be added as they become available; the XSPEC-user merely specifies a switch parameter to indicate which set of models is to be used in the fitting. We have also constructed tables of model spectra that account for relativistic effects and dipolar magnetic field and temperature variations on the surface of the neutron star. These spectra are more realistic but also more model-dependent. They show significant smearing of spectral features compared to the models that assume a uniform magnetic field.

We thank Keith Arnaud for assistance in incorporating NSMAX into XSPEC and the anonymous referee for helping to improve the clarity of the paper. WCGH

FIG. 14.— The same as in Fig. 13 but with  $\theta_m = 90^\circ$ .

appreciates the use of the computer facilities at the Kavli Institute for Particle Astrophysics and Cosmology. WCGH is supported by NASA LTSA grant NAG5-13032. The work of AYP is supported in part by FASI (Rosnauka) grant NSh-2600.2008.2 and by RFBR grants 05-02-22003 and 08-02-00837. The work of GC is supported in part by CNRS grant PICS 3202.

## REFERENCES

- Aguilera, D. N., Pons, J. A., & Miralles, J. A. 2007, *A&A*, submitted (arXiv:0710.0854)
- Alcock, C. & Illarionov, A. 1980, *ApJ*, 235, 534
- Arnaud, K. A. 1996, in *ASP Conf. Ser. 101, Astronomical Data Analysis Software and Systems V*, ed. G. H. Jacoby & J. Barnes (San Francisco: ASP), 17
- Beloborodov, A.M. 2002, *ApJL*, 566, L85
- Bezchastnov, V. G., Pavlov, G. G., Shibanov, Yu. A., & Zavlin, V. E. 1996, in *AIP Conf. Proc. 384, Gamma-Ray Bursts*, ed. C. Kouveliotou, M. F. Briggs, & G. J. Fishman (Woodbury: AIP), 907
- Brown, E. F., Bildsten, L., & Chang, P. 2002, *ApJ*, 574, 920
- Bulik, T. & Miller, M. C. 1997, *MNRAS*, 288, 596
- Chang, P., & Bildsten, L. 2003, *ApJ*, 585, 464
- Chang, P., Arras, P., & Bildsten, L. 2004, *ApJ*, 616, L147
- Gänsicke, B.T., Braje, T.M., & Romani, R.W. 2002, *A&A*, 386, 1001
- Geppert, U., Küker, M., & Page, D. 2006, *A&A*, 457, 937
- Ginzburg, V. L., & Ozernoi, L. M. 1965, *Sov. Phys. JETP*, 20, 689
- Greenstein, G., & Hartke, G. J. 1983, *ApJ*, 271, 283
- Haberl, F. 2007, *Ap&SS*, 308, 181
- Haensel, P., Potekhin, A. Y., & Yakovlev, D. G. 2007, *Neutron Stars I: Equation of State and Structure* (New York: Springer)
- Heinke, C. O., Rybicki, G. B., Narayan, R., & Grindlay, J. E. 2006, *ApJ*, 644, 1090
- Ho, W. C. G. 2007, *MNRAS*, 380, 71
- Ho, W. C. G. & Lai, D. 2001, *MNRAS*, 327, 1081
- Ho, W. C. G. & Lai, D. 2003, *MNRAS*, 338, 233
- Ho, W. C. G. & Lai, D. 2004, *ApJ*, 607, 420
- Ho, W. C. G., Lai, D., Potekhin, A. Y., & Chabrier, G. 2003, *ApJ*, 599, 1293
- Kaspi, V. M., Roberts, M. S. E., Harding, A. K. 2006, in *Compact Stellar X-ray Sources*, ed. W. Lewin & M. van der Klis (Cambridge: Cambridge University Press), 279
- Lai, D. 2001, *Rev. Mod. Phys.*, 73, 629
- Lai, D. & Salpeter, E. E. 1997, *ApJ*, 491, 270
- Lloyd, D. A. 2003, *MNRAS*, submitted (arXiv:astro-ph/0303561)

- McClintock, J. E., Narayan, R., & Rybicki, G. B. 2004, *ApJ*, 615, 402
- Mészáros, P. 1992, *High-Energy Radiation from Magnetized Neutron Stars* (Chicago: University of Chicago Press)
- Mészáros, P., Novick, R., Chanan, G. A., Weisskopf, M. C., Szentgyörgyi, A. 1988, *ApJ*, 324, 1056
- Miller, M. C., 1992, *MNRAS*, 255, 129
- Mori, K. & Hailey, C. J. 2002, *ApJ*, 564, 914
- Mori, K. & Hailey, C. J. 2006, *ApJ*, 648, 1139
- Mori, K. & Ho, W. C. G. 2007, *MNRAS*, 377, 905
- Özel, F., 2001, *ApJ*, 563, 276
- Page, D. 1995, *ApJ*, 442, 273
- Pavlov, G. G. & Zavlin, V. E. 2000, *ApJ*, 529, 1011
- Pavlov, G. G., Shibano, Yu. A., Ventura, J., & Zavlin, V. E., 1994, *A&A*, 289, 837
- Pavlov, G. G., Shibano, Yu. A., Zavlin, V. E., & Meyer, R. D. 1995, in *Lives of the Neutron Stars*, ed. M. A. Alpar, Ü. Kiziloğlu, & J. van Paradijs (Boston: Kluwer), 71
- Pechenick, K. R., Ftaclas, C., & Cohen, J. M. 1983, *ApJ*, 274, 846
- Pérez-Azorín, J. F., Pons, J. A., Miralles, J. A., & Miniutti, G. 2006, *A&A*, 459, 175
- Potekhin, A. Y. 1994, *J. Phys. B*, 27, 1073
- Potekhin, A. Y. & Chabrier, G. 2003, *ApJ*, 585, 955
- Potekhin, A. Y. & Chabrier, G. 2004, *ApJ*, 600, 317
- Potekhin, A. Y. & Pavlov, G. G. 1997, *ApJ*, 483, 414
- Potekhin, A. Y., Chabrier, G., & Shibano, Yu. A. 1999, *Phys. Rev. E*, 60, 2193
- Potekhin, A. Y., Chabrier, G., & Yakovlev, D. G. 2007, *Ap&SS* 308, 353 (corrected version – arXiv:astro-ph/0611014v3)
- Potekhin, A. Y., Lai, D., Chabrier, G., & Ho, W. C. G. 2004, *ApJ*, 612, 1034
- Potekhin, A. Y., Yakovlev, D. G., Chabrier, G., & Gnedin, O. Y. 2003, *ApJ*, 594, 404
- Rajagopal, M. & Romani, R. W., 1996, *ApJ*, 461, 327
- Rajagopal, M., Romani, R. W., & Miller, M. C., 1997, *ApJ*, 479, 347
- Reisenegger, A., Benguria, R., Prieto, J. P., Araya, P. A., & Lai, D. 2007, *A&A*, 472, 233
- Romani, R. W., 1987, *ApJ*, 313, 718
- Shibano, Yu. A., Zavlin, V. E., Pavlov, G. G., & Ventura, J. 1992, *A&A*, 266, 313
- van Adelsberg, M., & Lai, D. 2006, *MNRAS*, 373, 1495
- van Kerkwijk, M. H. & Kaplan, D.L. 2007, *Ap&SS*, 308, 191
- Woods, P. M. & Thompson, C. 2006, in *Compact Stellar X-ray Sources*, ed. W. Lewin & M. van der Klis (Cambridge: Cambridge University Press), 547
- Zane, S., & Turolla, R. 2006, *MNRAS*, 366, 727
- Zane, S., Turolla, R., & Treves, A., 2000, *ApJ*, 537, 387
- Zane, S., Turolla, R., Stella, L., & Treves, A. 2001, *ApJ*, 560, 384
- Zavlin, V. E. 2007, in *Proc. 363 WE-Heraeus Seminar on Neutron Stars and Pulsars*, ed. W. Becker, Springer Lecture Notes, in press (arXiv:astro-ph/0702426)
- Zavlin, V. E., Pavlov, G. G., Shibano, Yu. A., & Ventura, J. 1995a, *A&A*, 297, 441
- Zavlin, V. E., Shibano, Yu. A., & Pavlov, G. G. 1995b, *Astron. Lett.*, 21, 149
- Zavlin, V. E., Pavlov, G. G., & Shibano, Yu. A., 1996, *A&A*, 315, 141